
UNCERTAINTY QUANTIFICATION AND SENSITIVITY ANALYSIS FOR DIGITAL TWIN ENABLING TECHNOLOGY FOR ACCIDENT TOLERANT FUEL: APPLICATION FOR BISON FUEL PERFORMANCE CODE

A PREPRINT

Kazuma Kobayashi

Department of Nuclear Engineering and Radiation Science
Missouri University of Science and Technology
Rolla, MO 65409, USA

James Daniell

Department of Nuclear Engineering and Radiation Science
Missouri University of Science and Technology
Rolla, MO 65409, USA

Dinesh Kumar

Department of Mechanical Engineering
University of Bristol
Bristol BS8 1TR, UK

Susmita Naskar

¹Faculty of Engineering and Physical Sciences
University of Southampton
Southampton, UK

Souvik Chakraborty

Department of Applied Mechanics
School of Artificial Intelligence
Indian Institute of Technology Delhi
Hauz Khas - 110016, New Delhi, India

Kyle Paaren

Fuel Development, Performance, and Qualification
Idaho National Laboratory
Idaho Falls, ID 83415

Joseph Graham

Department of Nuclear Engineering and Radiation Science
Missouri University of Science and Technology
Rolla, MO 65409, USA

Syed Alam

Department of Nuclear Engineering and Radiation Science
Missouri University of Science and Technology
Rolla, MO 65409, USA

November 28, 2022

ABSTRACT

To understand the potential of intelligent confirmatory tools, the U.S. Nuclear Regulatory Committee (NRC) and U.S. Department of Energy (DOE) initiated a future-focused research project to assess the regulatory viability of machine learning (ML) and artificial intelligence (AI)-driven Digital Twins (DTs) for nuclear power applications. Advanced accident tolerant fuel (ATF) is one of the priority focus areas of the DOE and NRC. DTs integrated with ML/AI models have the potential to transform the nuclear energy sector in the coming years by incorporating risk-informed decision-making into the Accelerated Fuel Qualification (AFQ) process for ATF. A DT framework can offer game-changing yet practical and informed solutions to the complex problem of qualifying advanced ATFs. However, novel ATF technology suffers from a couple of challenges, such as (i) Data unavailability; (ii) Lack of data, missing data, and data inconsistencies; (iii) Model uncertainty. These challenges must be

resolved to gain the "trust" in DT framework development. In addition, DT-enabling technologies consist of three major areas: (i) modeling and simulation (M&S), covering uncertainty quantification (UQ), sensitivity analysis (SA), data analytics through ML/AI, physics-based models, and data-informed modeling, (ii) Advanced sensors/instrumentation, and (iii) Data & information management. UQ and SA are important segments of DT-enabling technologies to ensure trustworthiness, which need to be implemented to meet the DT requirement. Considering the regulatory standpoint of the modeling and simulation (M&S) aspect of DT, UQ and SA are paramount to the DT framework's success in terms of multi-criteria and risk-informed decision-making. In this study, the adaptability of polynomial chaos expansion (PCE) based UQ/SA in a non-intrusive method in BISON was investigated to ensure M&S aspects of the AFQ for ATF. This study introduces the ML-based UQ and SA methods while exhibiting actual applications to the finite element-based nuclear fuel performance code.

Keywords Machine Learning · Uncertainty Quantification · Sensitivity Analysis · Nuclear Power System · Fuel Performance Code · BISON

1 Introduction

Since the Fukushima nuclear accident in 2011, the environment surrounding the nuclear sector has changed significantly. There is a renewed focus on extending the service life of existing reactors, optimizing their operation, and increasing their efficiency. Accordingly, the development of accident tolerant fuels (ATFs) is one of the prime topics Almutairi et al. [2022]. Against these trends, U.S. Nuclear Regulatory Commission (NRC) advocated the application of digital twin (DT) technology to the nuclear field as an area of future research Yadav et al. [2021].

According to the NCR Yadav et al. [2021], the following potential benefits are expected due to DT in nuclear power plants: increased operational efficiencies, enhanced safety and reliability, reduced errors, faster information sharing, and better prediction. However, DT is an entirely new concept in the nuclear field, and the current stage of development is to identify the goals to be achieved and the technical issues to be addressed.

DT can be categorized by purpose, but the components are the same as followings: visualization, data processing, system update, prediction, and decision-making. In this context, "visualization" is used for preparing the virtual asset of a physical system and visualizing it on the computer. It is the foundation for building DT. This is similar to conventional simulation; imagine commercial software such as computer-aided design (CAD). Second, "data processing" is responsible for transferring the physical system's sensor data to the digital assets on the computer. Large systems such as nuclear reactors are expected to have a large number of sensors and data size and therefore require the construction of an appropriate database. The third "system update" clearly differs between DT and traditional simulation. A typical simulation predicts the system state at a given time, assuming that the system parameters are known. However, the objective of DT is to monitor and predict system conditions over a long time scale from the start of operation of that system to its shutdown (e.g., from months to years). It means that the system parameters themselves must be treated as a function of their system operation time, and their values must be updated as time evolves. Obtaining the system parameters at a given time is generally classified as an *inverse* problem, and the "update" handles the sequence of updating the obtained values at the next time step. The "prediction" predicts the system state using the above-mentioned updated system parameters. This process is a *forward* problem to solve for the system state, and the user can select any solvers according to the information they want to obtain. For example, for industrial products such as automobiles and aircraft, commercial FEA tools such as ABAQUS and ANSYS or in-house codes owned by each vendor would be an option. The final "decision-making" makes decisions about system maintenance, modifications, requests for maintenance, etc., based on the results of the previous forecasting module Kobayashi et al. [2022a], Kobayashi and Alam [2022], Kobayashi et al. [2022b]. This is challenging since it involves not only the design values of the system but also the restrictions imposed by national and international conventions. For example, consider an automobile as a system. Even if the driving performance is at the expected value, the vehicle must meet each country's exhaust gas emission regulations. Therefore, even if the same system is adopted, changing the decision-making module becomes a point of caution. All of these modules are essential, but in a nuclear system, the prediction tools are independent for each of their applications. In this study, the nuclear fuel performance evaluation code BISON is assumed to be one of the prediction tools in nuclear DT, and its potential applications are explored.

BISON is a finite element-based nuclear fuel performance code developed by Idaho National Laboratory (INL). It can be used with several fuel types, such as metallic rod (U-Pu-Zr) and plate fuel (U-10Mo), TRISO particle fuel, and fuel rods for light water reactors (UO₂) Hales et al. [2016], Idaho National Laboratory [a]. BISON is built on the Multiphysics Object-Oriented Simulation Environment (MOOSE) framework Permann et al. [2020].

For both 2D axisymmetric and 3D geometries, BISON can solve thermomechanical and species diffusion fully coupled equations. Temperature and burnup-dependent thermal properties, fission product swelling, densification, thermal and irradiation creep, fracture, and fission gas production/release are all capable of modeling, as well as how they interconnect with one another through tensor mechanics Hales et al. [2016]. For clad materials, plasticity, radiation growth, fuel cladding chemical interaction (FCCI), damage mechanics, and thermal and radiation creep models are used in addition to general material properties. There are also models that represent mechanical contact, gap heat transfer, change in gap/plenum pressure with plenum volume, gas temperature, and accumulation of fission gas Hales et al. [2016]. BISON is used to evaluate the condition of nuclear fuel pellets and cladding during reactor operation and is expected to be adopted as a predictive tool in nuclear system DT. However, the prediction is based on system parameters inferred from sensor data to obtain the system state. In reality, no sensor (for temporal synchronization within DT) exists with perfect accuracy, and uncertainties exist in its data. Therefore, quantifying the impact of uncertain input values on system response is a prerequisite for prediction tools Verma et al. [2022], Kobayashi et al. [2022c].

It is important to address that the DT-enabling technologies consist of three major areas Yadav et al. [2021]: (i) M&S, covering uncertainty quantification (UQ), sensitivity analysis (SA), data analytics through ML/AI, physics-based models, and data-informed modeling, (ii) Advanced sensors/instrumentation, and (iii) Data & information management. However, UQ and SA are important segments of DT-enabling technologies, and these need to be implemented in BISON to meet the DT requirement. In this study, the adaptability of polynomial chaos expansion (PCE) based UQ/SA in a non-intrusive method in BISON was investigated to ensure M&S aspects of the AFQ for ATF.

2 Uncertainty quantification using polynomial chaos

The polynomial chaos expansion (PCE) is a UQ technique that has already displayed potential for stochastic simulations. Mean, variance, higher-order moments, and probability density functions can be used to characterize variables, and the output solution Kumar et al. [2016, 2020a].

Orthogonal polynomials are polynomial classes that are orthogonal to one another in terms of a weight function. Popular orthogonal polynomials utilized in PC-based stochastic applications include Hermite polynomials, Laguerre polynomials, Jacobi polynomials, and Legendre polynomials. Orthogonality means:

$$\int_{\xi} \psi_i(\xi)\psi_j(\xi)W_{\xi}(\xi)d\xi = \langle \psi_i\psi_j \rangle = \delta_{ij} \langle \psi_i^2 \rangle \quad (1)$$

where $W_{\xi}(\xi)$ is the probability distribution (or weighting function) of the random variable ξ , δ_{ij} is the Kronecker delta, $\psi_i(\xi)$ are basis functions, and $\langle \psi_i\psi_j \rangle$ represents the inner product. Jacobi polynomials are implemented as default basis functions. The Jacobi polynomials are defined by Rodrigues' formula:

$$P_n^{(\alpha,\beta)}(z) = \frac{(-1)^n}{2^n n!} (1-z)^{-\alpha} (1+z)^{-\beta} \frac{d^n}{dz^n} \{ (1-z)^{\alpha} (1+z)^{\beta} (1-z^2)^n \} \quad (2)$$

with the constraints of $\alpha, \beta > -1$. Also, the orthogonality can be produced by:

$$\int_{-1}^1 P_n^{(\alpha,\beta)}(z)P_m^{(\alpha,\beta)}(z)(1-z)^{\alpha}(1+z)^{\beta} dz = \frac{2^{\alpha+\beta+1}}{2n+\alpha+\beta+1} \frac{\Gamma(n+\alpha+1)\Gamma(n+\beta+1)}{\Gamma(n+\alpha+\beta+1)} \delta_{n,m} \quad (3)$$

with the beta density $w(z) = (1-z)^{\alpha}(1+z)^{\beta}$ on $[-1, 1]$. By setting the parameters $\alpha = \beta = 0$ in this study, the Jacobi polynomials are modified to Legendre polynomials as follows:

$$P_n(z) = \frac{1}{2^n n!} \frac{d^n}{dz^n} (z^2 - 1)^n \quad (4)$$

The shapes of the Jacobi and Legendre polynomials are illustrated in Figure 1.

It is possible to separate deterministic and non-deterministic orthogonal polynomials in PCMs. For instance, the decomposition of a random variable $u(x, \xi)$ is:

$$u(x, \xi) = \sum_{i=0}^P u_i(x)\psi_i(\xi) \quad (5)$$

where $u_i(x)$ are the deterministic expansion coefficients and $P + 1$ is the total number of terms in the expansion. The mean of $u(x)$ can be written as:

$$E[u] = u_0 \quad (6)$$

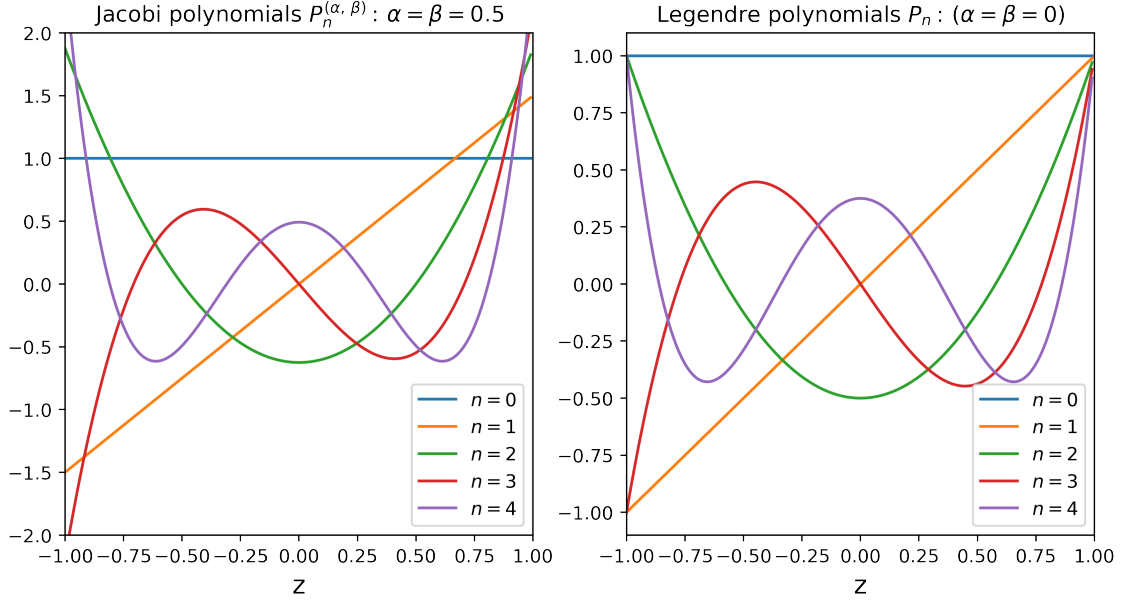


Figure 1: Example of 1D Jacobi polynomials and Legendre polynomials. n represents the order of polynomials.

and the variance as:

$$E[(u - E[u])^2] = \sigma_u^2 = \sum_{i=1}^P u_i^2 \langle \psi_i^2 \rangle \quad (7)$$

Typically there are 20 or more unknown parameters utilized in simulations since the PCE replaces each parameter with an additional set of unknown parameters (say 6 original parameters resulting in 120 parameters after PCE). High-dimensional stochastic problems require exponentially more computational power. This is known as the "curse of dimensionality" and is the primary drawback of PCM methods. For this reason, the development of efficient stochastic models for the analysis of uncertainty in complex industrial applications is of great interest Kumar et al. [2016].

2.1 Multi-dimensional polynomials

Building multi-dimensional polynomials from one-dimensional polynomials is necessary to study the impact of stochastic variables on final solutions. The multi-dimensional PCE of order p can be expressed in terms of 1D polynomials. For demonstration, a 2D PCE of order $p = 3$ is chosen.

When the set of 1-dimensional orthogonal polynomials of PC order 3 is defined as $\{\Psi_0, \Psi_1, \Psi_2, \Psi_3\}$, a 2D stochastic quantity $u(\xi_1, \xi_2)$ is expressed as a combination of the polynomial functions and coefficients.

$$\begin{aligned} u(\xi_1, \xi_2) = & u_{00}\Psi_0 \\ & + u_{10}\Psi_1(\xi_1) + u_{01}\Psi_1(\xi_2) \\ & + u_{20}\Psi_2(\xi_1) + u_{11}\Psi_1(\xi_1)\Psi_2(\xi_2) + u_{02}\Psi_2(\xi_2) \\ & + u_{30}\Psi_3(\xi_1) + u_{21}\Psi_2(\xi_1)\Psi_1(\xi_2) + u_{12}\Psi_1(\xi_1)\Psi_2(\xi_2) + u_{03}\Psi_3(\xi_2). \end{aligned} \quad (8)$$

For a set of multi-dimensional independent variables, $\xi = (\xi_1, \dots, \xi_n)$, the probability density function (PDF) can be defined by the following:

$$\mathbf{W}(\xi) = \prod_{i=1}^n W_i(\xi_i) \quad (9)$$

where $W_i(\xi_i)$ is the individual PDF of the random variable ξ_i Kumar et al. [2016, 2020a]. The sum of the polynomial terms $P + 1$ in Eq. 5 can be expressed with the polynomial order (p) and number of input variables (n) as:

$$P + 1 = \frac{(p + n)!}{p!n!} \quad (10)$$

Therefore, the sum of the polynomial terms ($P + 1 = 10$) can be computed ($p = 3, n = 2$).

2.2 Regression method to estimate PC coefficients

One common way to determine the unknown set of polynomial coefficients is by regression analysis. Regression analysis is a set of statistical procedures used to estimate the relationship between a dependent variable and one or more independent variables in a statistical method. In the most typical type of regression analysis, known as linear regression, the line that most closely matches the data is found. This method is often used in data analysis and in surrogate modeling methods such as Gaussian processes Kobayashi and Alam [2022].

Walters' regression-based non-intrusive polynomial chaos method computes polynomial coefficients Kumar et al. [2020a], Walters [2003]. In the sampling-based regression method, the unknown variables are written as the polynomial expansions of those variables. The approximate PCE for the stochastic quantity of interest, $u(x; \xi)$, is as follows:

$$u(x; \xi) = \sum_{i=0}^P u_i(x) \psi_i(\xi) \quad (11)$$

Using m samples ($\xi^j = \{\xi_1, \dots, \xi_{n_s}\}^j; j = 1, \dots, m$) shown by the PDF $\mathbf{W}(\xi)$ from Eq. 9 and the corresponding model output $u(x; \xi^j)$, this system can be represented as a matrix equation:

$$\begin{bmatrix} \psi_0(\xi^1) & \psi_1(\xi^1) & \cdots & \psi_P(\xi^1) \\ \psi_0(\xi^2) & \psi_1(\xi^2) & \cdots & \psi_P(\xi^2) \\ \vdots & \vdots & \ddots & \vdots \\ \psi_0(\xi^m) & \psi_1(\xi^m) & \cdots & \psi_P(\xi^m) \end{bmatrix} \begin{bmatrix} u_0(x) \\ u_1(x) \\ \vdots \\ u_P(x) \end{bmatrix} = \begin{bmatrix} u(x; \xi^1) \\ u(x; \xi^2) \\ \vdots \\ u(x; \xi^m) \end{bmatrix} \quad (12)$$

or in matrix notation

$$[A]\{u\} = \{b\} \quad (13)$$

The objective is to solve this equation for $\{u\}$; it can be expressed using matrix notation with the assumption of $m > P + 1$:

$$\{u\} = ([A]^T [A])^{-1} [A]^T \{b\} \quad (14)$$

By combining Eqs. 6, 7, 9 and 14, the mean and variance of system outputs can be quantitatively evaluated by considering the uncertainty of input variables. In the preceding system of equations, the matrix $[A]$ is referred to as the design matrix because it contains information about the polynomial values that the design samples Kumar et al. [2016]. In least-squares-based regression, the design matrix $[A]$ plays a pivotal role. Therefore, the sampling method and the number of samples significantly affect the instancing of the design matrix. Various sampling strategies, such as the Latin hypercube Helton and Davis [2003], the Sobol sequence Sobol' [1967], and random sampling Etikan and Bala [2017] can be used to build the design matrix. The influence of various sampling techniques and the number of total samples was studied in the previous works Kumar et al. [2020b], Hosder et al. [2006], Kumar et al. [2021, 2022], and it was concluded that more than twice as many samples, $2(P + 1)$, as PC coefficients are needed to ensure accuracy.

2.3 Global Sensitivity Analysis

Although the system response due to uncertain input variables is quantified using UQ methods, the contribution from the individual inputs should also be considered. Sobol sensitivity is one of the global sensitivity analysis methods Sobol [2001]. In this method, the system response, $u(x)$, is decomposed by associating with the input $x = (x_1, \dots, x_n)$:

$$u(x) = u_0 + \sum_{s=1}^n \sum_{i_1, \dots, i_s}^n u_{i_1 \dots i_s}(x_{i_1}, \dots, x_{i_s}) \quad (15)$$

where $i \leq i_1 < \dots < i_s \leq n$. Also, Eq. 15 can be expressed using analysis of variance (ANOVA) Cardinal and Aitken [2013] representation,

$$u(x) = u_0 + \sum_i u_i(x_i) + \sum_{i < j} u_{ij}(x_i, x_j) + \dots + u_{12\dots n}(x_1, x_2, \dots, x_n). \quad (16)$$

under the condition of

$$\int_0^1 u_{i_1, \dots, i_s}(x_{i_1}, \dots, x_{i_s}) dx_k = 0 \quad (17)$$

where $k = i_1, \dots, i_s$.

The individual term can be analytically described as:

$$\int u(x) dx = u_0, \quad (18)$$

$$\int u(x) \prod_{k \neq i} dx_k = u_0 + u_i(x_i), \quad (19)$$

$$\int u(x) \prod_{k \neq i, j} dx_k = u_0 + f_i(x_i) + f_j(x_j) + f_{ij}(x_i, x_j). \quad (20)$$

Based on these descriptions, Sobol Sobol [2001] introduced a method for calculating the variance of a response function, $u(x)$, by assuming it to be square integrable. The variances are expressed as follows:

$$V = \int u^2(x) dx - u_0^2 \quad (21)$$

and

$$V_{i_1 \dots i_s} = \int u_{i_1 \dots i_s}^2 dx_{i_1} \dots dx_{i_s}. \quad (22)$$

The relationship between the above variances is

$$V = \sum_{s=1}^n \sum_{i_1 < \dots < i_s} V_{i_1 \dots i_s}. \quad (23)$$

Finally, the ratios of variances are called Sobol indices.

$$S_{i_1 \dots i_s} = \frac{V_{i_1 \dots i_s}}{V} \quad (24)$$

where S_i is a measure of the first order sensitivity, which expresses the effect of the total variance produced by the uncertainties from input variable x . It is known that the Sobol indices can be acquired from PCE Kumar et al. [2020b]. Therefore, a set of the PCEs and the system response are acquired, with which the Sobol indices can be computed.

3 Method

This section explains the material models and problem setup. In order to demonstrate the uncertainty quantification method and sensitivity analysis of BISON code, a sample problem is prepared. The materials employed in the problems are UO_2 and SiC/SiC . *Note that the purpose of this study is to apply the PCE technique to BISON and to simplify the system; the mass density and thermal conductivity of the UO_2 fuel and SiC/SiC cladding are fixed.*

As mentioned above, in this study, the built-in thermal conductivity models of UO_2 and SiC/SiC incorporated in BISON were not used, however available models are briefly introduced below.

3.1 UO_2 Models

Material models are available in BISON for the following material properties of UO_2 : thermal conductivity, specific heat, elasticity tensor, creep, thermal expansion, and swelling.

The thermal conductivity and specific heat capacity for UO_2 can be computed using empirical models: Fink-Lucuta Fink [2000], Lucuta et al. [1996], Halden Lanning et al. [2005], NFIR A. Marion (NEI) letter dated June 13, 2006 to H. N. Berkow (USNRC/NRR) [2006], Lyon [2015], Modified NFI Ohira and Itagaki [1997], Ronchi-Staicu Ronchi et al. [2004], Staicu et al. [2014], and Toptan Toptan et al. [2020]. These models incorporate the effects of temperature, porosity, burnup, stoichiometry, and gadolinium content. Unlike the thermal conductivity model, which offers both semi-empirical and analytical options, the specific heat capacity is available only as an empirical model. The specific heat, C_p (J/mol-K), is expressed by

$$C_p = \frac{K_1 \theta^2 \exp(\frac{\theta}{T})}{T^2 [\exp(\frac{\theta}{T}) - 1]^2} + K_2 T + \frac{Y K_3 E_D}{2RT^2} \exp\left(-\frac{E_D}{RT}\right) \quad (25)$$

where T is the temperature (K), Y is the oxygen-to-metal ratio, R is the universal gas constant (8.3145 J/mol-K), and the coefficients are empirically properties. The default constant values are listed in Table 1. In this study, the thermal conductivity and specific heat are set to be the user-defined and the empirical model (Eq. 25), respectively.

Table 1: Constant parameters for UO_2 specific heat retrieved from Luscher et al. [2015]

Constant	UO_2	Units
K_1	296.7	J/kg-K
K_2	2.43×10^{-2}	J/kg-K ²
K_3	8.745×10^7	J/kg
θ	535.285	K
Y	2.0	-
E_D	1.577×10^5	J/mol

For the elasticity tensor model, the predefined constant values of Young's modulus and Poisson's ratio are set at $E = 2.0 \times 10^{11}$ Pa and $\nu = 0.345$ Idaho National Laboratory [b], respectively. There is no change in these values across the material's entire temperature range of use with this setting.

The creep of UO_2 is approximated by utilizing the MATPRO FCREEP model Allison et al. [1993]. This model treats a combination of thermal creep and irradiation creep, and it is expressed as follows:

$$\dot{\epsilon} = \frac{A_1 + A_2 \dot{F}}{(A_3 + D)G^2} \sigma \exp\left(-\frac{Q_1}{RT}\right) + \frac{A_4}{(A_6 + D)} \sigma^{4.5} \exp\left(-\frac{Q_2}{RT}\right) + A_7 \dot{F} \sigma \quad (26)$$

where $\dot{\epsilon}$ is the creep rate (1/s), σ is the effective stress (Pa), T is the temperature (K), D is the fuel density (percent of theoretical), G is the grain size (μm), \dot{F} is the volumetric fission rate (fissions/ $\text{m}^3\text{-s}$), Q_i are the activation energies (J/mol), and R is the universal gas constant (8.3143 J/mol-K). The constant parameters employed in Eq. 26 are listed in Table 2. The activation energies in Eq. 26 are defined as functions of the oxygen-to-metal ratio x by the following expressions:

$$\begin{aligned} Q_1 &= 74.829 f(x) + 301.762 \\ Q_2 &= 83.143 f(x) + 469.191 \end{aligned} \quad (27)$$

where the function $f(x)$ is defined as

$$f(x) = \frac{1}{\exp\left(-\frac{20}{\ln(x-2)} - 8\right) + 1} \quad (28)$$

For the thermal expansion of UO_2 , the MATPRO FTHEXP function was selected. This model can compute dimensional changes in unirradiated fuel pellets as a temperature-dependent function, and handles UO_2 and PuO_2 in solid, liquid, or

Table 2: Constant parameters for the UO₂ creep model Allison et al. [1993]

Parameter	Value
A_1	0.3919
A_2	1.3100×10^{-19}
A_3	-87.7
A_4	2.0391×10^{-25}
A_6	-90.5
A_7	3.7226×10^{-35}

both phases and includes solid-liquid expansion Allison et al. [1993]. The equation for the thermal expansion of UO₂ in solid phase is expressed by

$$\frac{\Delta L}{L_0} = P_1 T - P_2 + P_3 \exp\left(-\frac{P_{ED}}{k_B T}\right) \quad (29)$$

where $\Delta L/L_0$ is the linear strain caused by thermal expansion, T is the temperature (K), P_{ED} is the energy of formation of a defect (J), k_B is the Boltzmann's constant (1.38×10^{-23} J/K). The constants P_{ED} and P_i are determined by the fuel material. Values for UO₂ and PuO₂ are listed in Table 3.

Table 3: Constant parameters used in MATPRO FTHEXP function Allison et al. [1993]

Parameter	UO ₂	PuO ₂	Units
P_1	1.0×10^{-5}	9.0×10^{-6}	K ⁻¹
P_2	3.0×10^{-3}	2.7×10^{-3}	-
P_3	4.0×10^{-2}	7.0×10^{-2}	-
P_{ED}	6.9×10^{-20}	7.0×10^{-20}	J

Fuel volume swelling is caused by densification and fission products. For densification, the ESCORE model Rashid et al. [2004] is selected. It is given by

$$\left(\frac{\Delta V}{V_0}\right)_{den} = \Delta\rho_0 \left[\exp\left(\frac{Bu \ln(0.01)}{C_D Bu_D}\right) - 1 \right] \quad (30)$$

where $\Delta V/V_0$ is the densification strain, $\Delta\rho_0$ is the total densification, Bu is the burnup (fissions/atoms-U), and Bu_D is the burnup at which densification is complete (fissions/atoms-U). C_D represents the temperature dependence and changes value at 750 °C. Hence, during the simulation, the parameter C_D is automatically switched as follows:

$$C_D = \begin{cases} 7.235 - 0.0086(T - 25)/500 & (T < 750 \text{ °C}) \\ 1.0 & (T \geq 750 \text{ °C}) \end{cases} \quad (31)$$

Fission products also contribute to fuel swelling, and they can be classified into two types: (1) solid fission products and (2) gaseous fission products. For both kinds of swellings, the MATPRO models are applicable. The model for solid fission product (sf_p) is provided as a function of burnup:

$$\Delta V_{sf_p} = 5.577 \times 10^{-5} \rho \Delta Bu \quad (32)$$

and for gaseous fission product (gf_p):

$$\Delta V_{gf_p} = 1.96 \times 10^{-31} \rho \Delta Bu (2800 - T)^{11.73} \exp(-0.0162(2800 - T)) \exp(-0.0178 \rho Bu) \quad (33)$$

where ΔV_{sf_p} and ΔV_{gf_p} represent the volumetric swelling increment, ρ is the density (kg/m³) of fuel and T is the temperature in Kelvin.

3.2 SiC/SiC Models

Chemical Vapor Infiltrated SiC/SiC Composite (CVI SiC/SiC) is employed as a fuel cladding material in this study. The following built-in BISON models for CVI SiC/SiC are utilized: thermal conductivity, specific heat, elasticity tensor, thermal expansion, and volumetric swelling.

In BISON, there are three thermal conductivity models for SiC/SiC: Koyanagi Koyanagi et al. [2017], Stone Stone et al. [2015], and Combined models. The Koyanagi model is for unirradiated composite sic/sic and is derived from experimental thermal diffusivity data for tube-shaped samples. The Stone model is applicable to both irradiated and unirradiated composite sic/sic. The Stone model is unique in that it derives thermal conductivity as a function of temperature only, as opposed to the Koyanagi model, which gives thermal conductivity as a function of thermal diffusivity, specific heat, and density of composite sic/sic. The combined model allows one to incorporate the irradiation response from the Stone model into the Koyanagi model Idaho National Laboratory [b]. For the specific heat capacity (J/kg-K), the model of monolithic SiC is employed and it is given by

$$C_P = 925.65 + 0.3773T - 7.9259 \times 10^{-5}T^2 - \frac{3.1946 \times 10^7}{T^2} \quad (34)$$

where T is the temperature (K). In this study, the thermal conductivity and specific heat capacity are user-defined values for the monolithic SiC model (Eq. 34).

The Elasticity tensor of composite SiC/SiC is complex. In general, when SiC/SiC is used for cladding applications, it is considered to be orthotropic: 3D braided architecture with fibers along the axial direction and angles $\pm\theta$ from the axial direction of the cladding Idaho National Laboratory [b]. The material properties are affected by fiber orientation and porosity. Experimental works are ongoing to quantify these effects. In this work, as suggested by literature AZoNetwork [2022], we assumed Young's modulus of 90 GPa and Poisson's ratio of $\nu = 0.35$.

The strain due to thermal expansion is computed from the correlation reported by Koyanagi Koyanagi et al. [2017]. The linear thermal expansion coefficient (K^{-1}) is given as a function of temperature (K) as follows:

$$\alpha = 1.0 \times 10^{-6}(-0.7765 + 0.014350T - 1.2209 \times 10^{-5}T^2 + 3.8289 \times 10^{-9}T^3) \quad (35)$$

where the valid temperature range is $294 < T \leq 1273$. The thermal strain is computed incrementally using the average coefficient of thermal expansion across the time step given the incremental temperature change Idaho National Laboratory [b].

$$\epsilon_{th}^{curt} = \epsilon_{th}^{pre} + (T_{curt} - T_{pre}) \frac{\alpha_{curt} + \alpha_{pre}}{2} \quad (36)$$

where the superscript *curt* and subscript *pre* represent the current time step and previous time step, respectively. The simulation's reference temperature for no thermal expansion event must be set in BISON, with a temperature of 295 (K) employed in this study.

BISON utilizes the same volumetric swelling model as the monolithic SiC for composite SiC/SiC. Katoh model is one option that includes both temperature and neutron fluence effects Idaho National Laboratory [b]. The swelling strain is expressed as a differential equation of fast neutron fluence for this option Idaho National Laboratory [b], Stone et al. [2015]:

$$\frac{dS}{d\gamma} = k(T)\gamma^{-1/3} \exp\left(-\frac{\gamma}{\gamma_{sc}(T)}\right) \quad (37)$$

where S is the swelling strain, γ is the fast neutron fluence (cm^{-2}), $k(T)$ is a temperature-dependent rate constant, and $\gamma_{sc}(T)$ is a temperature-dependent characteristic fast neutron fluence. The following gives the two constants:

$$k(T) = 6.0631 \times 10^{-8}T^2 - 1.5904 \times 10^{-4}T + 0.10612 \quad (38)$$

and

$$\gamma_{sc}(T) = 6.7221 \times 10^{-12}T^4 - 1.3095 \times 10^{-8}T^3 + 9.4807 \times 10^{-6}T^2 - 2.7651 \times 10^{-3}T + 0.51801 \quad (39)$$

The Katoh model has an option for the number of steps in the incremental calculation of swelling in the low fluence region. In this study, it is set to 1000.

The summary of the built-in material models are listed in Table 4.

Table 4: List of the BISON built-in material models that were used in this research

Material	Physical quantity	BISON Function name	Reference
UO ₂	Thermal conductivity & heat capacity	HeatConductionMaterial ¹	Idaho National Laboratory [b]
	Elasticity tensor	UO2ElasticityTensor	Idaho National Laboratory [b]
	Stress	ComputeMultipleInelasticStress ²	Idaho National Laboratory [b]
	Creep	UO2CreepUpdate	Allison et al. [1993]
	Thermal expansion	UO2ThermalExpansionMATPROEigenstrain	Allison et al. [1993]
	Volumetric swelling	UO2VolumetricSwellingEigenstrain	Allison et al. [1993], Rashid et al. [2004]
SiC/SiC	Thermal conductivity & heat capacity	HeatConductionMaterial ¹	Idaho National Laboratory [b]
	Elasticity tensor	ComputeIsotropicElasticityTensor ³	Malvern [1969], Slaughter [2012]
	Stress	ComputeStrainIncrementBasedStress	Idaho National Laboratory [b]
	Thermal expansion	CompositeSiCThermalExpansionEigenstrain	Koyanagi et al. [2017]
	Volumetric Swelling	CompositeSiCVolumetricSwellingEigenstrain	Mieloszyk [2015]

¹ the setting of user-defined thermal conductivity in the BISON input file

² iteratively compute stress, internal parameters, and plastic strains

³ compute a constant isotropic elasticity tensor

3.3 Problem Setup

The model is composed of three regions: fuel, gap, and cladding. The overview of the system is shown in Figure 2, and the geometric parameters are listed in Table 5. The fuel pellet is UO₂, the gap is helium gas, and the cladding material is SiC/SiC. A heat transfer analysis of the system is performed. The parameters for the heat source and coolant channel are listed in Table 6. The simulation is performed using the Dirichlet boundary condition for the displacements, and two sets of pressure boundary conditions are applied: one from the coolant, which applies pressure to the exterior of the cladding, and another from the plenum pressure, which applies pressure to both the exterior and interior surfaces of the fuel and cladding interiorIdaho National Laboratory [c].

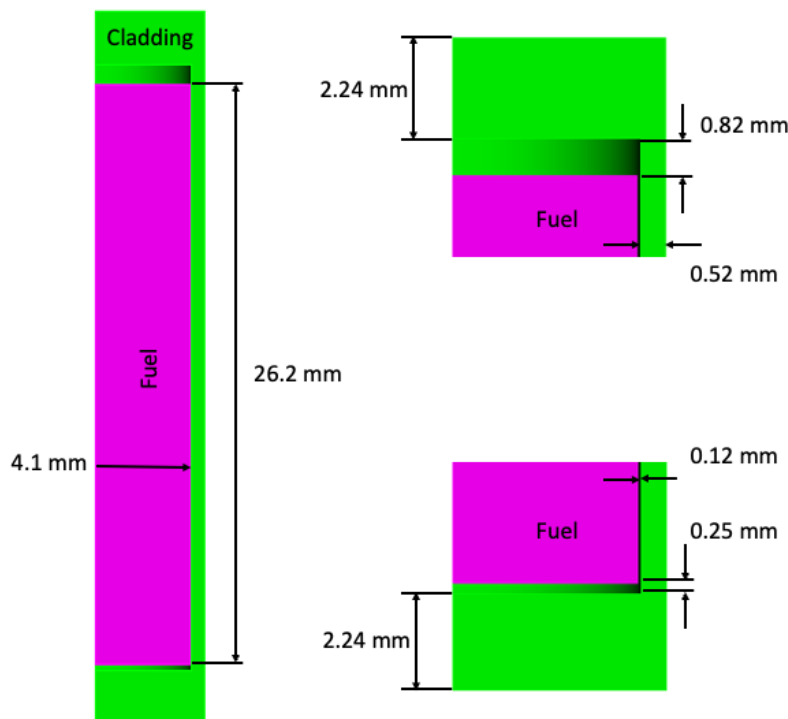


Figure 2: 3D geometry of a one-quarter fuel pin. A purple region represents a fuel pellet domain and a green region shows a cladding

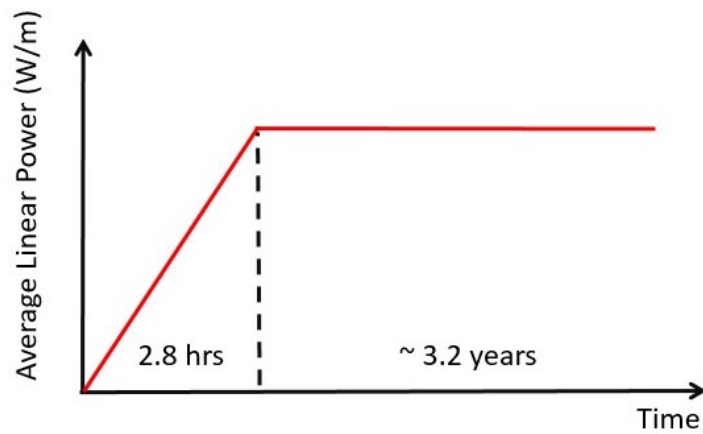
The rod power history is shown in Figure 3. The rod power is assumed³ to start rising and reach the maximum in 2.8 hours, and is kept for 3.2 years.

Table 5: Geometric parameters of fuel, gap, and cladding

Domain	Parameters	Values (mm)
(1) Fuel	radius	4.1
	height	26.2
(2) Gap	plenum	0.82
	radial	0.12
	axial	0.25
(3) Cladding	inner radius	4.22
	outer radius	4.74
	radial thickness	0.52
	axial thickness	2.24
	height	29.3

Table 6: Input parameters for the problem: heat source and coolant

Parameters	Values	Units
Fission energy	3.20×10^{-11}	J/fission
Coolant inlet temperature	580	K
Coolant inlet pressure	15.5	MPa
Coolant mass flux	3800	kg/m ² -sec
Rod diameter	9.48×10^{-3}	m
Fuel pin pitch	1.26×10^{-2}	m

Figure 3: Power history for the simulation. The peak value is 1.5×10^4 (W/m).

3.4 Input Variables

In this demonstration, the uncertain input variables were room temperature values of thermal conductivity and mass density of UO_2 and SiC/SiC . Since these values affect temperature, burnup, and fission gas functions, they must be updated at each calculation step. However, the purpose of this study is to introduce the implementation of the UQ method in BISON, input variables were set to static numbers.

All input variables are assumed to follow a Gaussian distribution with a 5% coefficient of variation, which is a standard deviation/mean. The values are listed in Table 7.

Table 7: List of input variables for fuels and SiC/SiC cladding

Domain	Input variables	Mean (RSD %)
		$\text{UO}_2 + \text{SiC/SiC}$
Fuel	thermal conductivity (W/mK) Wu and Yin [2022]	2.8 (5)
	density (kg/m^3) Wu and Yin [2022]	10430.0 (5)
Cladding	thermal conductivity (W/mK) Kowbel et al. [2000]	75 (5)
	density (kg/m^3) Kowbel et al. [2000]	2650.0 (5)

As it is mentioned in Sections 2.1 and 2.2, the sampling number should be greater than $2(P + 1)$ to ensure accuracy. In this problem, there are 4 input variables (n) and the polynomial order (p) of 3. Hence, the required sample number can be computed:

$$2(P + 1) = 2 \frac{(p + n)!}{p!n!} = 2 \frac{(3 + 4)!}{3!4!} = 70 \quad (40)$$

In order to ensure adequate over-sampling, 100 samples were generated for the UO_2 system using the Monte Carlo sampling method. The probability distribution functions (PDF) for $\text{UO}_2 + \text{SiC/SiC}$ is shown in Figure 4.

Figure 5 illustrates a series of tasks in the PCE methodology. The first task is the preparation of input variables, already described in Section 3.4. The second task is to prepare input files for BISON. Since 100 sets of four input variable pairs are used in this study, a similar number of corresponding BISON input files are prepared. The third task is to feed the prepared input files to BISON and compile calculation results. The fourth task is to compute a multi-dimensional polynomial function from the random variables used in the input variable preparation (Section 2.1). Tasks 3 and 4 yield the system matrix, and solving it for polynomial coefficients is the final task 5. The mean and variance of the output values are calculated using the coefficients and polynomial functions by Eqs. 6 and 7.

4 Results and Discussion

3D axisymmetric BISON simulations were performed to compute the average burnup, maximum cladding surface temperature, maximum fuel centerline temperature, cladding inner, fuel pellet volume, and plenum pressure. Figures 6 represent the mean values and single standard deviation confidence intervals obtained with the PCM. The individual contribution of input variables on the system response is quantified and expressed using the first order Sobol's sensitivity indices as shown in Figure 7.

Figure 6 (a) shows that the burnup and its uncertainty increase slowly up to 10^6 seconds, after which it increases rapidly with time additional. The Sobol indices indicate the fuel density affects the burnup in Figure 7 (a). It reflects that the fission rate is a function of uranium density.

The cladding surface and fuel centerline temperatures are shown in Figure 6 (b) and Figure 6 (c). They appear to follow the power history. Both temperatures increase and reach equilibrium conditions at 2.8 hours. The mean value and standard deviation of cladding surface temperature converged (RSD < 0.0%). In contrast, the fuel centerline shows significant fluctuations (RSD \sim 1.2%). Also, it is confirmed that the maximum cladding surface and fuel centerline temperatures do not exceed their melting point, UO_2 : 3138 (K) and SiC : 3003 (K). This remains true when the input uncertainties are taken into account. The effects of input variables on the cladding surface and fuel centerline are shown in Figure 7 (b) and Figure 7 (c). Figure 7 (b) reveals that the cladding surface temperature is affected by the fuel thermal conductivity, fuel density, and cladding thermal conductivity, respectively. In contrast, the dominant contributor to the fuel centerline temperature is only the thermal conductivity of the fuel pellet.

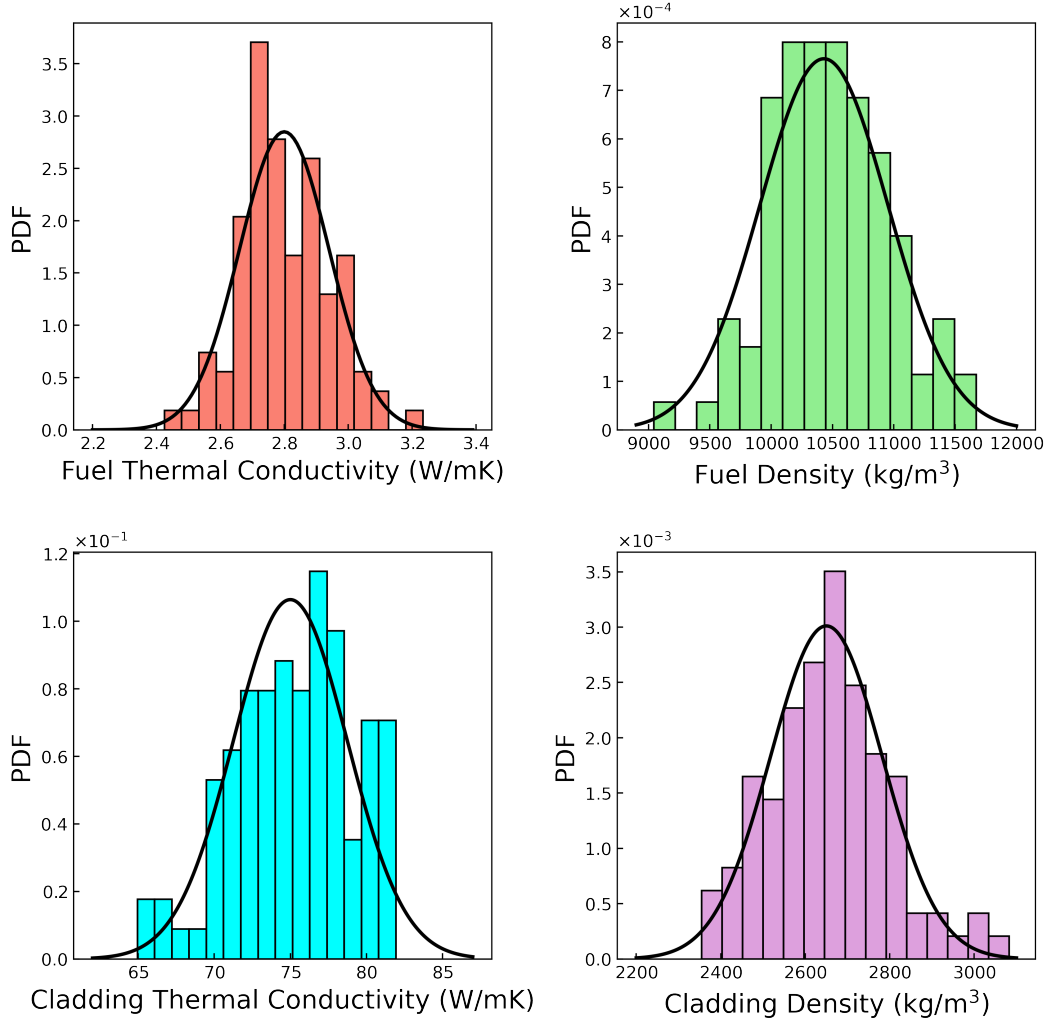


Figure 4: Probability distributions of input variables generated with the Monte Carlo sampling for $\text{UO}_2 + \text{SiC/SiC}$ setup

The volume changes of cladding inner region and fuel pellet are shown in Figure 6 (d) and Figure 6 (e). These two output values correlate with each other. The fuel volumetric swelling represented in Figure 6 (e) is a competitive process between densification and solid and gaseous fission product swellings. When the reactor starts, densification is the dominant process in the fuel pellet until 10^4 seconds (~ 2.8 hours). This period matches the power history, from zero power to the maximum power of 1.5×10^4 (W/m). During the period between 10^4 and $\sim 10^6$ seconds, a plateau region appears. It can be understood as the three competing processes reaching equilibrium due to the stabilization of burnup and temperature. The fission product swellings are dominant until $\sim 10^7$ seconds. After 10^7 seconds, densification becomes the dominant process again. As shown in Figure 6 (d), the impact of uncertain input variables on the cladding inner volume is not critical. However, Figure 7 (d) shows that cladding inner volume is sensitive to the cladding thermal conductivity. For the fuel volume change, the first contributor is the fuel thermal conductivity, and the second is fuel density, as shown in Figure 7 (e).

Figure 6 (f) shows the plenum pressure. The negative correlation between the plenum pressure and the fuel volume is apparent. As fuel volume decreases, plenum pressure rises. Conversely, as fuel volume rises, plenum pressure falls. The phenomena are particularly noticeable up to 10^4 seconds and around 10^7 seconds. As it is shown in Figure 7 (f), the plenum pressure is sensitive to the fuel density and thermal conductivity. This result matches that of fuel density as shown in Figure 7 (e).

Only uncertainties of the input variables were taken into account in this work. In other words, the confidence intervals (standard deviations) depicted in Figure 6 were likely underestimated since the code's inherent uncertainty was not taken into consideration. Notably, one must carefully consider the applicability of BISON's material modeling. Most built-in

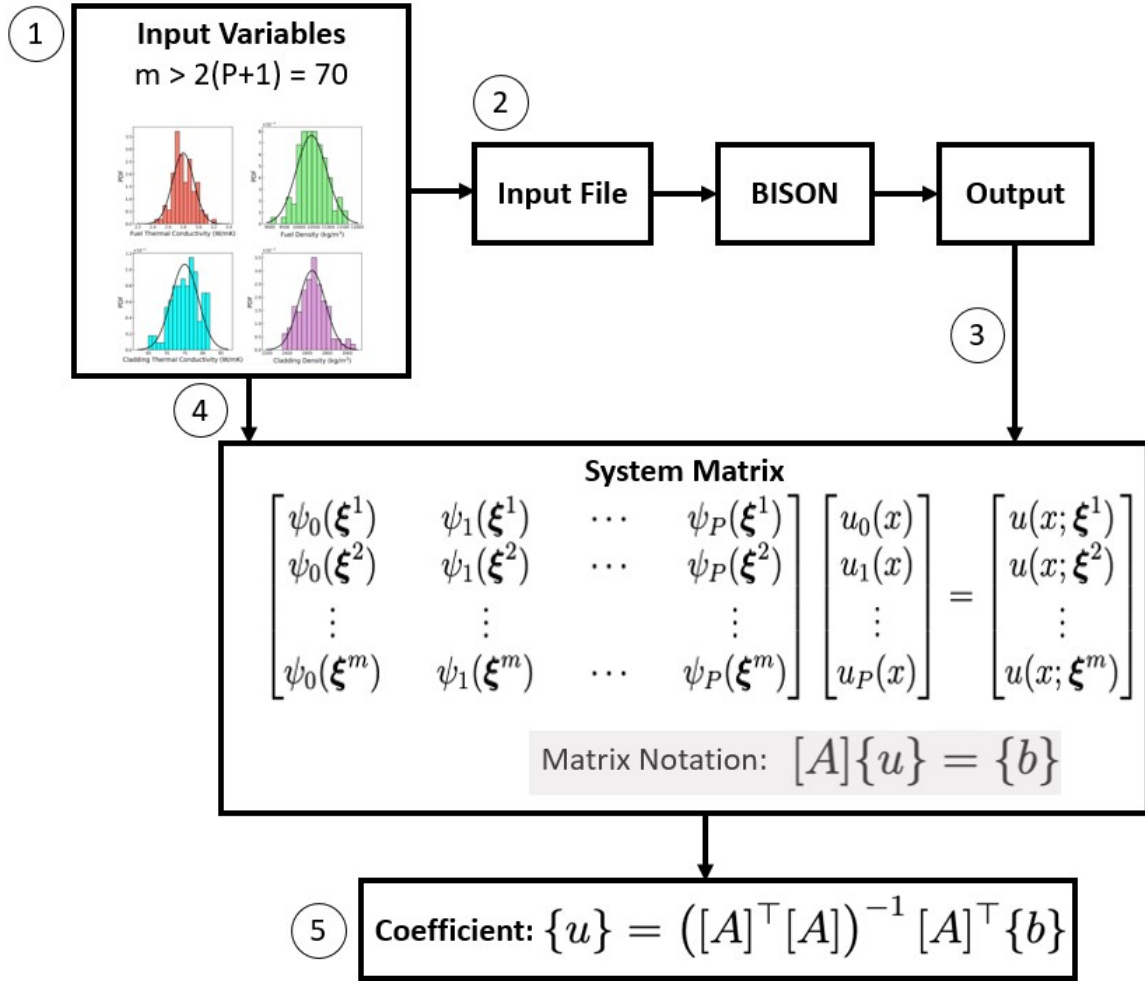


Figure 5: Flow chart of UQ analysis.

material models are prepared using empirical correlations, and their uncertainties are not utilized in the simulations. The model's validity is guaranteed in the case of established nuclear materials such as UO_2 , for which experimental data have been accumulated sufficiently. However, in simulations using innovative nuclear fuels and cladding materials, the validity and uncertainty of the empirical models will have a significant impact on the calculation results. Future research needs to quantify the impact on the final system outputs, assuming uncertainty in the input variables and the model.

5 Conclusion

DTs integrated with ML/AI models can help NRC and DOE to make risk-informed decision-making for the Accelerated Fuel Qualification process for the ATF. Among other components, uncertainty quantification and sensitivity analysis are two important segments of DT-enabling technologies to ensure trustworthiness. In this paper, uncertainty quantification and sensitivity analysis using polynomial chaos expansion was performed on the nuclear fuel performance code BISON. As uncertain input variables, material densities and thermal conductivities for UO_2 fuel and SiC/SiC cladding were employed. The impact of the input uncertainties on the burnup, cladding surface temperature, fuel centerline temperature, cladding inner volume, fuel volume, and plenum pressure was analyzed. It was demonstrated that the system output could be expressed in terms of mean and standard deviation even when uncertainties in the input variables are considered. The sensitivity analysis concluded that the material density and thermal conductivity of SiC/SiC cladding have little contribution to the output parameters except for the cladding's inner volume. It can be concluded that the methods presented in this study can provide more reliable calculation results to ensure the potential of BISON as a prediction tool in a DT for nuclear systems.

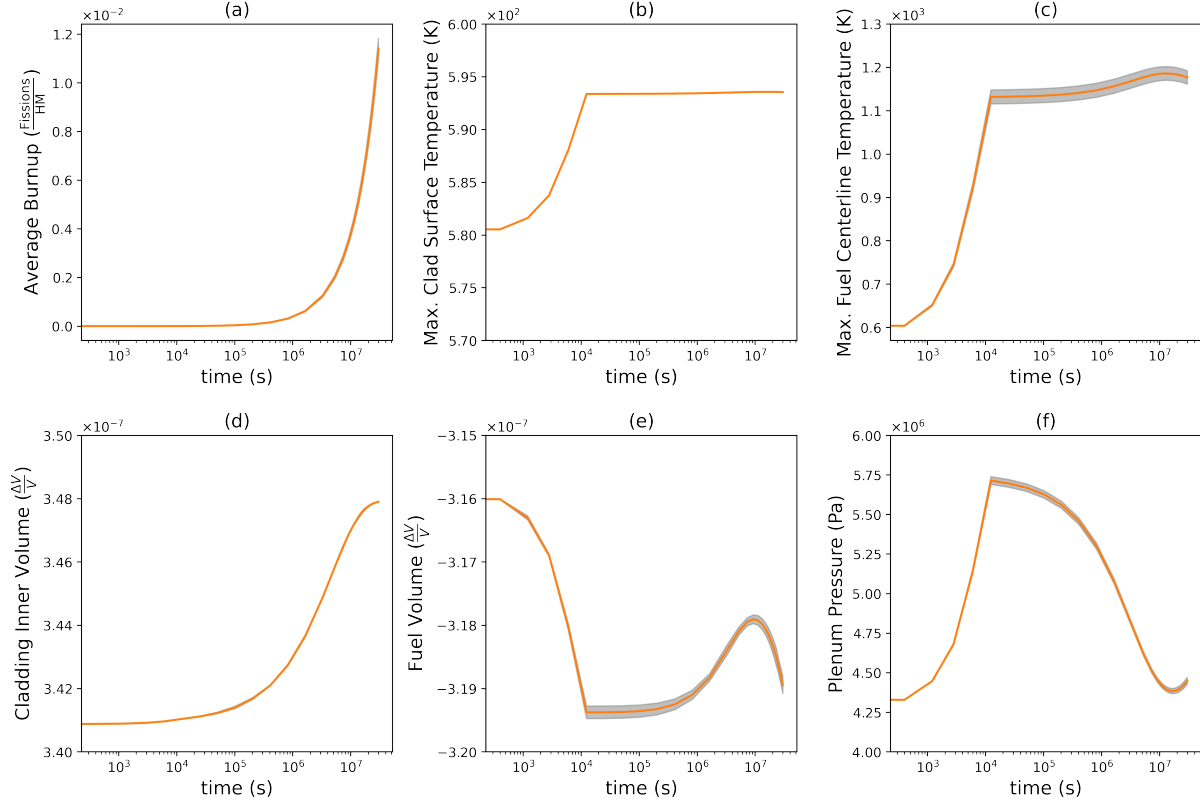


Figure 6: Results of the $\text{UO}_2+\text{SiC}/\text{SiC}$. The mean values are shown with solid orange lines, and the confidence intervals corresponding to 1 standard deviation are drawn as shadow regions. For all output variables, the mean and standard deviation were computed.

Future work will focus on implementing prediction algorithms for BISON to tackle the ATF challenges of data unavailability, lack of data, missing data, and data inconsistencies. In addition, Explainable AI (XAI)-Infused Trustworthy DT framework and development of update module by Solving the “Inverse Problem” for synchronizing the physical and DT leveraging BISON code will be performed.

Acknowledgement

The computational part of this work was supported in part by the National Science Foundation (NSF) under Grant No. OAC-1919789 and the High Performance Computing Center at Idaho National Laboratory, which is supported by the Office of Nuclear Energy of the U.S. Department of Energy and the Nuclear Science User Facilities under Contract No. DE-AC07-05ID14517.

References

- Bader Almutairi, Safwan Jaradat, Dinesh Kumar, Cameron S Goodwin, Shoaib Usman, Ayodeji Alajo, and Syed Bahuddin Alam. Weight loss and burst testing investigations of sintered silicon carbide under oxidizing environments for next generation accident tolerant fuels for smr applications. *Materials Today Communications*, 30:102958, 2022.
- Vaibhav Yadav, Vivek Agarwal, Andrei V Gribok, Ross D Hays, Adam J Pluth, Christopher S Ritter, Hongbin Zhang, Prashant K Jain, Pradeep Ramuhalli, Doug Eskins, et al. Technical challenges and gaps in digital-twin-enabling technologies for nuclear reactor applications, 2021.
- Kazuma Kobayashi, James Daniell, Shoaib Usman, Dinesh Kumar, and Syed Alam. Surrogate modeling-driven physics-informed multi-fidelity kriging: Path forward to digital twin enabling simulation for accident tolerant fuel. *Springer Nature Handbook of Smart Energy Systems*, arXiv preprint arXiv:2210.07164, 2022a.

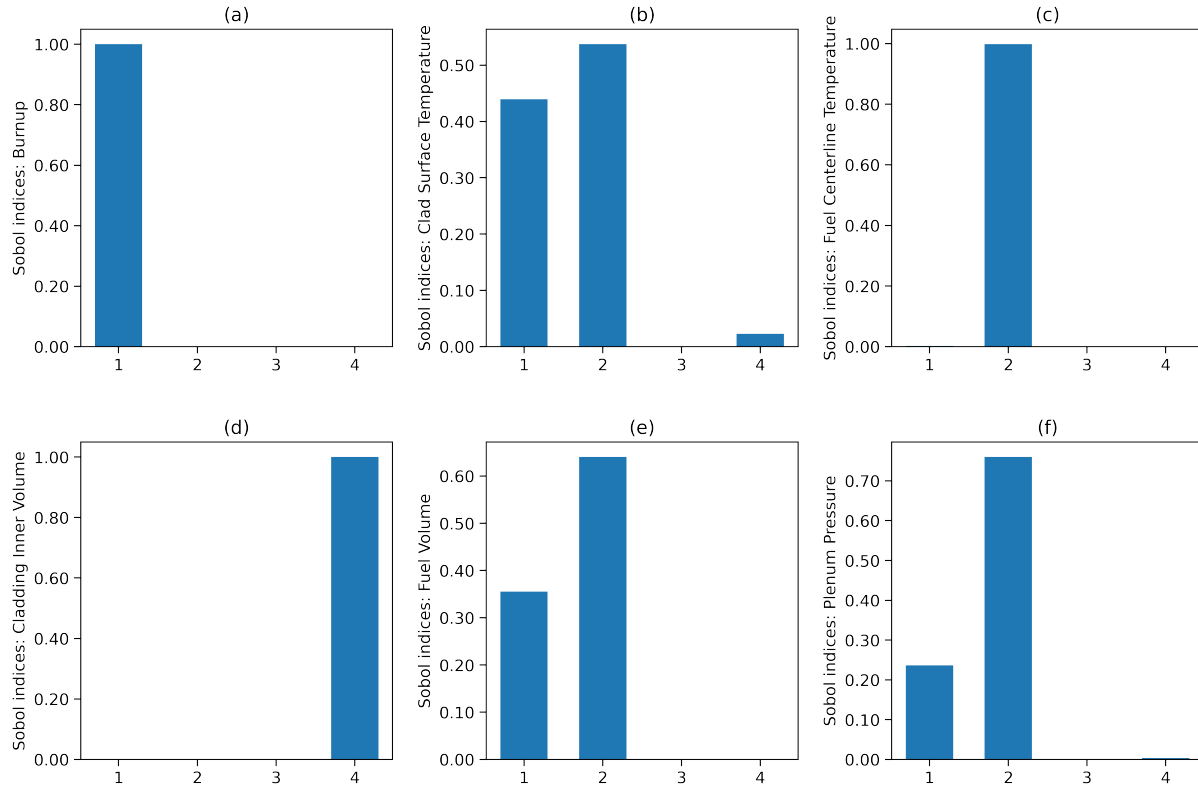


Figure 7: First order Sobol' sensitivity indices in the $\text{UO}_2 + \text{SiC/SiC}$ setup. The x-axis represents the index of input parameters, 1: fuel density, 2: fuel thermal conductivity, 3: cladding density, and 4: cladding thermal conductivity.

Kazuma Kobayashi and Syed Alam. Practical applications of gaussian process with uncertainty quantification and sensitivity analysis for digital twin for advanced nuclear fuel. In *Springer Handbook of Smart Energy System*. Springer Nature, 2022.

Kazuma Kobayashi, Dinesh Kumar, Matthew Bonney, Souvik Chakraborty, Kyle Paaren, and Syed Alam. Uncertainty quantification and sensitivity analysis for digital twin enabling technology: Application for bison fuel performance code. *Springer Nature Handbook of Smart Energy Systems*, arXiv preprint arXiv:2210.07541, 2022b.

JD Hales, RL Williamson, SR Novascone, G Pastore, BW Spencer, DS Stafford, KA Gamble, DM Perez, and W Liu. Bison theory manual the equations behind nuclear fuel analysis. Technical report, Idaho National Lab.(INL), Idaho Falls, ID (United States), 2016.

Idaho National Laboratory. BISON | A Finite Element-Based Nuclear Fuel Performance Code. <https://mooseframework.inl.gov/bison/index.html>, a. Accessed: 2022-08-30.

Cody J. Permann, Derek R. Gaston, David Andrš, Robert W. Carlsen, Fande Kong, Alexander D. Lindsay, Jason M. Miller, John W. Peterson, Andrew E. Slaughter, Roy H. Stogner, and Richard C. Martineau. MOOSE: Enabling massively parallel multiphysics simulation. *SoftwareX*, 11:100430, 2020. ISSN 2352-7110. doi:<https://doi.org/10.1016/j.softx.2020.100430>. URL <http://www.sciencedirect.com/science/article/pii/S2352711019302973>.

Richa Verma, Dinesh Kumar, Kazuma Kobayashi, and Syed Alam. Reliability-based robust design optimization method for engineering systems with uncertainty quantification. *Springer Nature Handbook of Smart Energy Systems*, arXiv preprint arXiv:2210.07521, 2022.

Kazuma Kobayashi, Shoaib Usman, Carlos Castano, Ayodeji Alajo, Dinesh Kumar, and Syed Alam. Data-driven multi-scale modeling and robust optimization of composite structure with uncertainty quantification. *Springer Nature Handbook of Smart Energy Systems*, arXiv preprint arXiv:2210.09055, 2022c.

Dinesh Kumar, Mehrdad Raisee, and Chris Lacor. An efficient non-intrusive reduced basis model for high dimensional stochastic problems in cfd. *Computers and Fluids*, 138:67–82, 2016. ISSN 00457930. doi:[10.1016/j.compfluid.2016.08.015](https://doi.org/10.1016/j.compfluid.2016.08.015). URL <http://dx.doi.org/10.1016/j.compfluid.2016.08.015>.

- D. Kumar, S. B. Alam, Dean Vučinić, and C. Lacor. *Uncertainty Quantification and Robust Optimization in Engineering*, pages 63–93. Springer Singapore, Singapore, 2020a. ISBN 978-981-13-9806-3. doi:10.1007/978-981-13-9806-3_3. URL https://doi.org/10.1007/978-981-13-9806-3_3.
- Robert Walters. Stochastic fluid mechanics via polynomial chaos. In *41st Aerospace Sciences Meeting and Exhibit*, page 413, 2003.
- Jon C Helton and Freddie Joe Davis. Latin hypercube sampling and the propagation of uncertainty in analyses of complex systems. *Reliability Engineering & System Safety*, 81(1):23–69, 2003.
- Il'ya Meerovich Sobol'. On the distribution of points in a cube and the approximate evaluation of integrals. *Zhurnal Vychislitel'noi Matematiki i Matematicheskoi Fiziki*, 7(4):784–802, 1967.
- Ilker Etikan and Kabiru Bala. Sampling and sampling methods. *Biometrics & Biostatistics International Journal*, 5(6): 00149, 2017.
- Dinesh Kumar, Yao Koutsawa, Gaston Rauchs, Mariapia Marchi, Carlos Kavka, and Salim Belouettar. Efficient uncertainty quantification and management in the early stage design of composite applications. *Composite Structures*, 251, nov 2020b. ISSN 02638223. doi:10.1016/j.compstruct.2020.112538.
- Serhat Hosder, Robert Walters, and Rafael Perez. A non-intrusive polynomial chaos method for uncertainty propagation in cfd simulations. In *44th AIAA aerospace sciences meeting and exhibit*, page 891, 2006.
- Dinesh Kumar, Syed Bahauddin Alam, Tuhfatur Ridwan, and Cameron S Goodwin. Quantitative risk assessment of a high power density small modular reactor (smr) core using uncertainty and sensitivity analyses. *Energy*, 227:120400, 2021.
- Dinesh Kumar, Mariapia Marchi, Syed Bahauddin Alam, Carlos Kavka, Yao Koutsawa, Gaston Rauchs, and Salim Belouettar. Multi-criteria decision making under uncertainties in composite materials selection and design. *Composite Structures*, 279:114680, 2022.
- Ilya M Sobol. Global sensitivity indices for nonlinear mathematical models and their monte carlo estimates. *Mathematics and computers in simulation*, 55(1-3):271–280, 2001.
- Rudolf N Cardinal and Michael RF Aitken. *ANOVA for the behavioral sciences researcher*. Psychology Press, 2013.
- J. K. Fink. Thermophysical properties of uranium dioxide. *Journal of Nuclear Materials*, 279(1):1–18, 2000. ISSN 0022-3115.
- P.G. Lucuta, Hj. Matzke, and I.J. Hastings. A pragmatic approach to modelling thermal conductivity of irradiated UO₂ fuel: Review and recommendations. *Journal of Nuclear Materials*, 232(2-3):166–180, 1996. ISSN 0022-3115. doi:10.1016/S0022-3115(96)00404-7. URL <http://www.sciencedirect.com/science/article/pii/S0022311596004047>.
- D. D. Lanning, C. E. Beyer, and K. J. Geelhood. Frapcon-3 updates, including mixed-oxide fuel properties. Technical Report NUREG/CR-6534, Vol. 4 PNNL-11513, Pacific Northwest National Laboratory, 2005.
- A. Marion (NEI) letter dated June 13, 2006 to H. N. Berkow (USNRC/NRR). Safety Evaluation by the Office of Nuclear Reactor Regulation of Electric Power Research Institute (EPRI) Topical Report TR-1002865, "Topical Report on Reactivity Initiated Accidents: Bases for RIA Fuel rod Failures and Core Coolability Criteria". <http://pbadupws.nrc.gov/docs/ML0616/ML061650107.pdf>, 2006.
- W. F. Lyon. Summary report: Gd thermal conductivity model updates. Technical Report ANA-P1400138-TN03 Rev. 2, Anatech Corp., 2015.
- K. Ohira and N. Itagaki. Thermal conductivity measurements of high burnup UO₂ pellet and a benchmark calculation of fuel center temperature. In *Proceedings of the American Nuclear Society Meeting on Light Water Reactor Fuel Performance*, page 541, Portland, Oregon, Mar 2 to Mar 6, 1997.
- C Ronchi, M Sheindlin, D Staicu, and M Kinoshita. Effect of burn-up on the thermal conductivity of uranium dioxide up to 100.000 mwdt< sup>- 1. *Journal of Nuclear Materials*, 327:58–76, 2004. doi:10.1016/j.jnucmat.2004.01.018.
- D Staicu, VV Rondinella, et al. Effect of burn-up on the thermal conductivity of uranium-gadolinium dioxide up to 100 GWd/tHM. *Journal of Nuclear Materials*, 453:259–268, 2014. doi:10.1016/j.jnucmat.2014.07.006.
- A. Toptan, G. Pastore, R. L. Williamson, J. D. Hales, and S. R. Novascone. Engineering-scale modeling of thermal conductivity in BISON for UO₂ and Gd bearing UO₂ fuels. *submitted to Journal of Nuclear Materials*, 2020.
- WJ Luscher, KJ Geelhood, and IE Porter. Material property correlations: Comparisons between FRAPCON-4.0, FRAPTRAN-2.0, and MATPRO. Technical Report PNNL-19417 Rev. 2, Pacific Northwest National Laboratory, 9 2015.

- Idaho National Laboratory. BISON-Specific Input Syntax and Reference Manual. https://mooseframework.inl.gov/bison/syntax/bison_only_index.html, b. Accessed: 2022-08-30.
- C. M. Allison, G. A. Berna, R. Chambers, E. W. Coryell, K. L. Davis, D. L. Hagrman, D. T. Hagrman, N. L. Hampton, J. K. Hohorst, R. E. Mason, M. L. McComas, K. A. McNeil, R. L. Miller, C. S. Olsen, G. A. Reymann, and L. J. Siefken. SCDAP/RELAP5/MOD3.1 code manual, volume IV: MATPRO-A library of materials properties for light-water-reactor accident analysis. Technical Report NUREG/CR-6150, EGG-2720, Idaho National Engineering Laboratory, 1993.
- Y Rashid, R Dunham, and R Montgomery. Fuel Analysis and Licensing Code: FALCON MOD01. Technical report, Electric Power Research Institute, December 2004.
- T. Koyanagi, Y. Katoh, G. Singh, and M. Snead. SiC/SiC cladding materials properties handbook. Technical Report ORNL/TM-2017/385, Oak Ridge National Laboratory, 2017.
- J. G. Stone, R. Schleicher, C. P. Deck, G. M. Jacobsen, H. E. Khalifa, and C. A. Back. Stress analysis and probabilistic assessment of multi-layer sic-based accident tolerant nuclear fuel cladding. *Journal of Nuclear Materials*, 466: 682–697, 2015.
- AZoNetwork. Properties: Silicon carbide (sic) properties and applications, Nov 2022. URL <https://www.azom.com/properties.aspx?ArticleID=42>.
- Lawrence E Malvern. *Introduction to the Mechanics of a Continuous Medium*. Prentice-Hall, 1969.
- William S Slaughter. *The Linearized Theory of Elasticity*. Springer Science & Business Media, 2012.
- Alexander Mieloszyk. *Assessing thermo-mechanical performance of ThO₂ and SiC clad light water reactor fuel rods with a modular simulation tool*. PhD thesis, Massachusetts Institute of Technology, September 2015. <http://hdl.handle.net/1721.1/103660>.
- Idaho National Laboratory. Layered 1D LWR Rod Tutorial: BISON. https://mooseframework.inl.gov/bison/tutorials/layered1d_tutorial.html, c. Accessed: 2022-08-30.
- Xuezhi Wu and Bangyue Yin. Mechanism and properties of uo₂-graphene composite fuel prepared by in situ synthesis. *Crystals*, 12(2):230, 2022.
- W Kowbel, CA Bruce, KL Tsou, K Patel, JC Withers, and GE Youngblood. High thermal conductivity sic/sic composites for fusion applications. *Journal of Nuclear Materials*, 283:570–573, 2000.